

A Functionalised Nickel Cyclam Catalyst for CO₂ Reduction: Electrocatalysis, Semiconductor Surface Immobilisation and Light-Driven Electron Transfer

Gaia Neri,^a James J. Walsh,^a Calum Wilson,^b Anna Reynal,^c Jason Y. C. Lim,^c Xiaoe Li,^c Andrew J. P. White,^c Nicholas J. Long,^c James R. Durrant^c and Alexander J. Cowan^{b*}

The immobilisation of electrocatalysts for CO₂ reduction onto light harvesting semiconductors is proposed to be an important step towards developing more efficient CO₂ reduction photoelectrodes. Here, we report a low cost nickel cyclam complex covalently anchored to a metal oxide surface. Using transient spectroscopy we validate the role of surface immobilisation on enhancing the rate of photoelectron transfer. Furthermore [Ni(1,4,8,11-tetraazacyclotetradecane-6-carboxylic acid)]²⁺ (2**) is shown to be a very active electrocatalyst in solution.**

The photoelectrochemical reduction of CO₂ to products such as carbon monoxide, formic acid and methanol is receiving intense interest.^{1,2} When coupled to a water oxidation photocatalyst, light driven CO₂ reduction offers a sustainable route to carbon-based fuels from renewable feedstock. However, to date, the efficiency of such approaches has remained unfeasibly low and significant challenges remain including high electron-hole recombination yields, low selectivities towards CO₂ and the use of high cost materials and solvents.

Photoelectrochemical reduction of CO₂ in water is particularly challenging, as competitive proton reduction occurs at similar potentials.³ A promising approach to obtaining higher selectivity towards CO₂ reduction over H₂ production and increased solar to fuel efficiencies is to introduce a molecular electrocatalyst with a high selectivity towards CO₂.⁴ Numerous studies have explored the use of photocathodes to drive electrocatalysis in solution.⁵ Immobilisation of the electrocatalyst directly onto the photocathode surface to form a hybrid photoelectrode is also receiving increasing interest due to anticipated improvements in the rate of charge transfer to the molecular catalyst and in the stability and recyclability of the system.⁶ Immobilisation of a molecular catalyst either within a polymer or by electropolymerisation has been explored in several studies,^{7,8} including using [Re(bpy)(CO)₃Br] and [Co(bpy)₃]²⁺, with marked improvements in photoelectrochemical activity towards CO₂ being achieved. A series of studies^{9,10} explored the electropolymerisation of ruthenium electrocatalysts onto InP and GaP photoelectrodes with an overall solar to fuel efficiency of 0.14 % being reported for a SrTiO₃/InP/Ru device for the production of formate from water and CO₂. In contrast to the number of polymer-immobilised systems, few examples of directly anchored molecular catalysts are known, despite offering potential advantages over the control of the catalyst binding modes, which is highly desirable for optimising charge transfer at the semiconductor/catalyst interface. In 2010, Sato *et al.*^{6,11} reported the immobilisation of a ruthenium-based molecular electrocatalyst modified with carboxylic acid or phosphonic acid binding groups onto p-type N-Ta₂O₅ for use as a photocatalyst in CH₃CN. Significantly this study showed that the photocatalytic activity of the hybrid material far exceeded that of the two-components simply mixed in solution, with related transient absorption spectroscopy (TAS) measurements identifying charge transfer from the semiconductor to the immobilised electrocatalyst as a potentially significant factor.¹² Recently Ishitani *et al.* reported that [Ru{4,4'-CH₂PO₃H₂}-2,2'-bipyridine}(CO)₂Cl₂] immobilised on g-C₃N₄ is an active photocatalyst for reducing CO₂ to formic acid with a selectivity of > 80 % and a turnover number (TON) of > 200.¹³ The same group has also explored the binding of ruthenium catalysts to TaON for CO₂ reduction.¹⁴

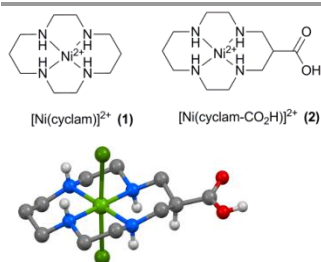


Figure 1: (a) [Ni(cyclam)]²⁺ (**1**) was functionalised on the carbon backbone with a carboxylic acid group to yield (**2**) for anchoring to metal oxide electrodes. (b) X-ray structure of **2**. H atoms, except for those bound to N or O, are emitted for clarity (details in ESI).

To the best of our knowledge, all of the examples of directly immobilised CO₂ molecular electrocatalysts on light absorbing semiconductors have either employed high cost metal centres (e.g. Ru)⁶ or complete enzymes.¹⁵ Here we explore the covalent immobilisation of a low cost [Ni(cyclam)]²⁺ (cyclam = 1,4,8,11-tetraazacyclotetradecane, (**1**)) derivative to metal oxide photoelectrodes. [Ni(cyclam)]²⁺ and its derivatives are widely studied electrocatalysts due to their high stability and selectivity towards the reduction of CO₂ to CO in water on mercury electrodes.¹⁶⁻¹⁹ Furthermore this class of catalyst is weakly coloured ($\epsilon_{d-d} \sim 10-50$), thereby avoiding detrimental inner-filter effects when used as the catalyst in a sensitised photocatalytic system. Photocatalytic CO₂ reduction has been reported for solutions containing **1** and a molecular

photosensitiser such as $[\text{Ru}(\text{bpy})_3]^{2+}$ (where $\text{bpy} = 2,2'$ -bipyridyl),^{20, 21} and for supramolecular systems consisting of ruthenium polypyridyl complexes covalently linked to **1**.^{22, 23} $[\text{Ni}(\text{cyclam})]^{2+}$ has also been used in solution with a range of p-type photoelectrodes such as p-Si, p-GaP or p-GaAs,²⁴⁻²⁶ which demonstrates the viability of using derivatives of **1** as catalysts in a light-driven system.

The synthetic procedure for the dichloride salt of **2**, a $[\text{Ni}(\text{cyclam})]^{2+}$ complex modified with a carboxylic acid group for binding to metal-oxide surfaces, is described in the ESI. We identified functionalisation of the carbon backbone as an appropriate route as it is known that the presence of the quaternary N-H protons within **1** are critical in aiding CO_2 binding and catalysis, with functionalisation of the amine groups leading to decreased selectivity.^{27, 28} The single crystal X-ray structure of the complex (Fig. 1) shows the nickel centre to have a slightly distorted octahedral coordination geometry (*cis* angles in the range $85.51(8)^\circ$ to $95.01(8)^\circ$), with the two chlorine ligands occupying the axial sites. In the crystal, the complex assumes a *R,R,S,S* (*trans*-III) conformation.²⁹ In aqueous solution, **1** primarily adopts a square planar configuration; however, in contrast, UV/Vis studies of **2** (Fig. S8) indicate the presence of a mix of octahedral and square planar geometries in aqueous solutions.³⁰ In line with these observations, the $^1\text{H-NMR}$ for complex **2** in D_2O presents a mix of very broad and resolved peaks, characteristic of species exhibiting a degree of paramagnetism.

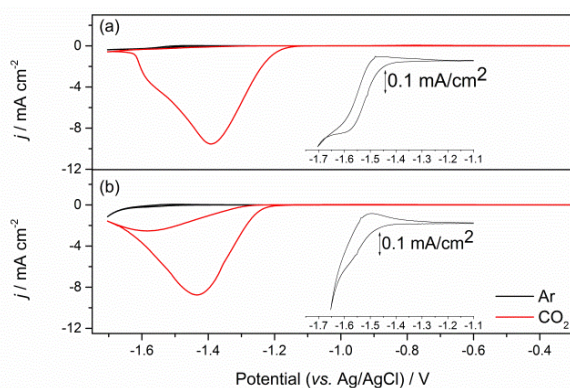


Figure 2: CV of ca. 1 mM solutions of **1** (a) and **2** (b) recorded in 0.1 M NaClO_4 at pH 5 purged with either argon (black line) or CO_2 (red line) recorded at 100 mVs^{-1} using a HMDE electrode (0.023 cm^2). The inset shows an expansion of the $\text{Ni}^{\text{II/I}}$ couple under argon, see also figure S4.

A very small number of studies have demonstrated that by careful control of the complex geometry it is possible to develop nickel cyclam derivative CO_2 reduction electrocatalysts with higher turnover frequencies and lower onset potentials;^{17, 18, 31} however more typically cyclam modification is found to have significant detrimental effects on the electrocatalytic activity towards CO_2 . Therefore it is interesting to also assess the electrocatalytic activity of **2** in solution. Cyclic voltammograms measured in 0.1 M aqueous NaClO_4 at pH 5 on a hanging drop mercury electrode (HMDE) are shown in Fig. 2 and Figs. S4-S6. On the HMDE the $\text{Ni}^{\text{II/I}}$ couple of **2** under argon appears at $-1.55 \text{ V vs. Ag/AgCl}$, close to that of the unmodified complex **1** ($-1.50 \text{ V vs. Ag/AgCl}$, inset in Fig. 2a)¹⁶, and a reversible $\text{Ni}^{\text{II/III}}$ couple for **2**, studied under argon on a glassy carbon working electrode at $0.43 \text{ V (vs. Fc/Fc}^+, \text{ ca. } 0.8 \text{ V vs Ag/AgCl)}$ is also noted (Fig. S1-S3). Under CO_2 a large increase in current is observed for both **1** and **2** at potentials close to that of $\text{Ni}^{\text{II/I}}$ under argon. In-line with the known activity of **1**, this is assigned to the electrocatalytic reduction of CO_2 to CO .¹⁶ Bulk electrolysis measurements carried out at $-1.4 \text{ V (vs. Ag/AgCl)}$ using an Hg-Au amalgam working electrode and 10^{-4} M solutions of **2** in 0.1 M NaClO_4 confirm that the large current enhancement under CO_2 is due to electrocatalytic CO_2 reduction to CO . An excellent selectivity towards CO_2 reduction is achieved with a $\text{CO}:\text{H}_2$ product ratio of $\sim 100:1$ as measured by headspace gas chromatography, with a combined Faradaic efficiency of 88 % and a turnover number for CO_2 reduction of 5.3 within 1 hour, indicating that modification of the carbon backbone of the cyclam ligand has not notably decreased the catalytic activity of **2** (Fig. S7). To further assess the electrocatalytic activity of **2** we have measured the ratio of the peak currents in the absence (i_p) and presence (i_{pc}) of the CO_2 substrate, which is a commonly used method to estimate electrocatalytic activity. Here we estimate $i_{pc}/i_p \sim 48$ for complex **2** which is slightly greater than the value for **1** ($i_{pc}/i_p \sim 31$). This could be taken to indicate enhanced catalytic activity, however it is important to note that the electrocatalysis onset is $\sim 50 \text{ mV}$ more cathodic for **2** (-1.27 V) than **1** (-1.22 V) and that accurate determination of i_p for **2** is complicated by the onset of hydrogen reduction at these negative potentials. Instead, in-line with a previous study on related complexes,¹⁸ a Tafel analysis was employed to provide a more detailed analysis of the electrocatalytic activity of **2** (Fig. 3). Analysis of the slow scan rate (2 mV s^{-1}) linear sweep voltammograms (LSVs) for **2** reveals that a significant pre-wave exists at overpotentials less than -0.6 V . Similar pre-waves have been observed for other modified nickel cyclams and they correlate to the adsorption and geometric reorganisation of the catalyst¹⁸. The slopes of the Tafel plots for **2** and **1** are found to be indistinguishable (56 mV/decade) for overpotentials between -0.61 and -0.99 V , the region confirmed where CO_2 reduction occurs (Fig. S7), further reinforcing that functionalisation of the cyclam structure has not detrimentally altered the electrocatalytic activity on mercury at pH 5.

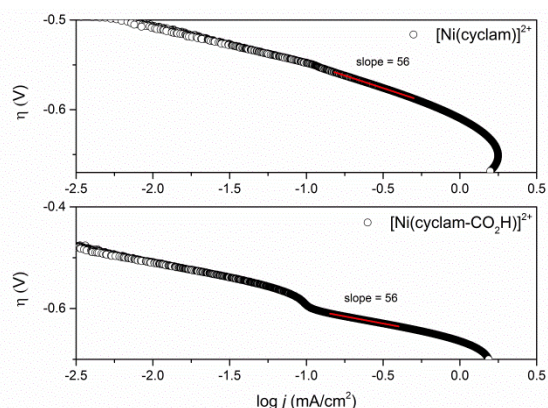


Figure 3: Plots of CO₂ reduction overpotential (pH = 5) vs. log of current density for catalysts **1** and **2**. Calculated from LSVs at 2 mV s⁻¹ in 0.1 M NaClO₄ electrolyte containing 1 × 10⁻⁴ M catalyst. Overpotentials were calculated from the thermodynamic potential for CO₂ reduction at pH = 5 (-0.41 V vs. NHE)¹⁸.

The presence of a suitable binding group on **2** permits the immobilisation of this catalyst onto metal oxide electrodes. Binding of **2** to semiconductor surfaces was performed by dip-coating nanocrystalline (nc) TiO₂ films (particle ϕ ~ 20 nm, film 3 μ m thick) on FTO glass in a 2 mM ethanolic solution of the catalyst for 48 hours. Catalyst uptake was evaluated and quantified by both measuring the decrease in absorbance of **2** in the soaking solution using UV-vis spectroscopy and through desorption of **2** from the surface using 1 M NaOH; typical experiments resulted in approximately 1000 molecules of **2** bound per TiO₂ nanoparticle (see ESI for calculations). The binding mode of **2** to nc-TiO₂ films was examined using FTIR spectroscopy (Fig. S9) which showed a clear shift in the ν (C=O) frequency of the carboxylic acid group of **2** when compared to that of the unbound solid sample. Careful analysis of the splitting of the asymmetric and symmetric stretching modes of the carboxylate group indicates that **2** is likely to be bound in a monodentate manner through this group to the TiO₂ surface.

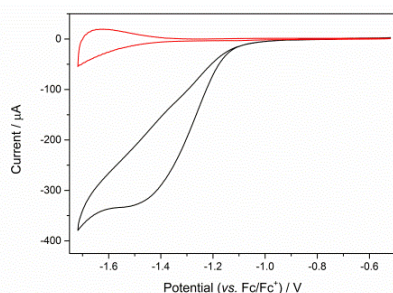


Figure 4: Cyclic voltammograms of nc-TiO₂ (red) and nc-TiO₂/2 (black) under argon in 0.1 M (But)₄NPF₆/MeCN. ν = 100 mV s⁻¹.

High surface area n-type semiconductors such as nc-TiO₂ have been explored as supports for reductive electrochemistry in the dark.³² In contrast to traditional conductive electrodes the redox species of interest is only observed at potentials close to, or negative of, the conduction band edge, *i.e.* when the semiconductor is no longer acting as an insulator.³² The energy of the TiO₂ conduction band (CB) edge is dependent upon both the solvent and the nature of the electrolyte ions studied.³³ In very dry aprotic solvents such as CH₃CN with (But)₄NPF₆ the CB potential is *ca.* -2.1 V (vs. Ag/AgCl),³³ sufficiently negative of the solution Ni^{III/I} potential of complex **2**. Here we have examined the electrochemistry of both **1** in solution with a TiO₂ electrode and of **2** immobilised on a TiO₂ electrode in CH₃CN. In the absence of a catalyst the CV of nc-TiO₂ in CH₃CN shows behaviour associated with the charging and discharging of trap states close to the conduction band edge, in line with previous reports, Fig. 4.^{34, 35} In contrast the electrochemical response of nc-TiO₂/2 is markedly different with the presence of a new reductive feature at -1.5 V (vs. Fc/Fc⁺), assigned to the reduction of the Ni^{II} of complex **2**, indicating that the catalyst remains electrochemically active on the semiconductor surface and that electron transfer from the semiconductor to the catalyst is achievable. The dependence of the current response on increasing scan rate (Fig. S12) indicates the absence of diffusion contributions, in line with a surface bound species. Controls experiments using a blank nc-TiO₂ electrode with either **1** or **2** in solution showed no features assignable to the Ni^{III/I} redox couple (Figs. S10, S11). Addition of CO₂ to the nc-TiO₂/2 system does lead to an initial increase in cathodic current, which may indicate electrocatalytic activity (Fig. S13), however the system is found to be insufficiently stable under CO₂ for bulk electrolysis experiments. Interestingly we also find that the potential of the Ni^{III/I} reduction of **2** on TiO₂ in CH₃CN (-1.4 V vs. Fc/Fc⁺, *ca.* -1.1 vs. Ag/AgCl) is shifted anodically compared with on a mercury electrode at pH 5 under argon, demonstrating a potential advantage of the immobilised system.

As the yield of photoelectron transfer across the catalyst/semiconductor interface is likely to be a critical factor in determining overall photocatalytic efficiency, it is important that the fundamental design rules controlling electron transfer to immobilised catalysts are explored. In order to identify if photoinduced electron transfer can occur from the semiconductor electrode to the immobilised cyclam complex **2**, we have studied TiO₂/2 in deaerated CH₃CN in the presence of triethanolamine (TEOA, 0.1 M) using TAS. TAS has been widely used to study the dynamics of photoelectrons and holes in

TiO₂ and it is known that conduction band photoelectrons have an absorption feature at wavelengths greater than 800 nm.³⁶ Following direct band gap excitation (355 nm, 6 ns) of nc-TiO₂ in the absence of either **1** or **2** with TEOA as the hole scavenger we observe a very long-lived transient absorption signal at 900 nm, that decays with $t_{50\%} = 0.8$ s, Fig. 5. This TAS signal is assigned to long-lived TiO₂ photoelectrons, as electron-hole recombination processes are suppressed due to the rapid scavenging of holes by TEOA.³⁷ In contrast, TAS experiments on TiO₂/**2** recorded under identical conditions show a rate of photoelectron decay ($t_{50\%} = 1.2$ ms) that is over two orders of magnitude faster than the control experiment of bare TiO₂. The rapid decay of the TiO₂ photoelectron signal indicates that efficient electron transfer from the TiO₂ to the immobilized catalyst occurs, in good agreement with our earlier electrochemical studies that demonstrated electron transfer from the conduction band of TiO₂ to the Ni^{III/I} couple is thermodynamically viable (Fig. 4). We have also carried out experiments of unmodified TiO₂ electrodes with complex **1** (*ca.* 1×10^{-4} M) in solution to explore the role of surface immobilisation on electron transfer kinetics and these data reveal that electron transfer from the metal oxide to [Ni(cyclam)]²⁺ in solution is an order of magnitude slower ($t_{50\%} = 20$ ms) than that observed for the hybrid TiO₂/**2** system, confirming that direct covalent immobilisation markedly improves the rate of photoelectron transfer to the electrocatalyst.

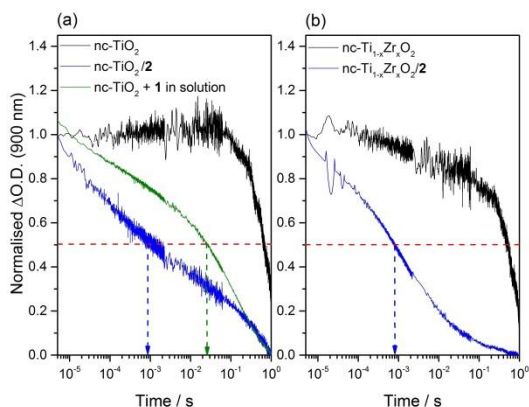


Fig. 5 Transient absorption decays of (a) unmodified TiO₂ (black), TiO₂/**2** (blue) and TiO₂ with 1×10^{-4} M in solution (green) and (b) Ti_{1-x}Zr_xO₂ (black) and Ti_{1-x}Zr_xO₂/**2** (blue) measured in CH₃CN with 0.1 M TEOA. The samples were excited at 355 nm ($350 \mu\text{J}/\text{cm}^2$) and probed at 900 nm. The samples were purged under N₂ for 15 min prior to measurements. A useful measure for the kinetics of the process is $t_{50\%}$ (dotted lines), which represents the time delay by which the yield of photoelectrons has dropped by 50% when compared to an initial concentration, here defined to be the photoelectron yield at 4 microseconds.

A very recent study on water splitting systems has shown that a key parameter controlling the rate of photoelectron transfer is the distance between the semiconductor and the catalytic core.³⁷ It is however also important to understand the role of the thermodynamic driving force on the rate of photoelectron transfer. Here we have also immobilised complex **2** on a mixed Ti_{1-x}Zr_xO₂ film ($x = 0.2$, see Figs. S14, S15). It has been previously shown that Ti_{1-x}Zr_xO₂ has a conduction band edge that is shifted by *ca.* 150 mV vs. nc-TiO₂ and this is also confirmed through spectroelectrochemical measurements, Fig. S16. TAS measurements on Ti_{1-x}Zr_xO₂/**2** show a marked increase in the rate of photoelectron decay ($t_{50\%} = 800 \mu\text{s}$) when compared to a Ti_{1-x}Zr_xO₂ film in the absence of the catalyst ($t_{50\%} = 500$ ms), indicating that photoelectron transfer to **2** from Ti_{1-x}Zr_xO₂ is occurring (Fig. S17). The faster rate of electron transfer in Ti_{1-x}Zr_xO₂/**2** is in-line with the increased thermodynamic driving force for electron transfer (~ 0.65 eV, Table S1) when compared to TiO₂/**2** (~ 0.5 eV, $t_{50\%} = 1.2$ ms), indicating that optimisation of the driving force for electron transfer to the catalyst is also an important parameter for achieving efficient charge transfer.

Conclusions

Here we report on the immobilisation of a low-cost nickel cyclam derivative to semiconductor materials with potential applications for high surface area electrochemistry and photoelectrochemical CO₂ reduction. To the best of our knowledge this represents the first example of a photo-driven nickel cyclam covalently anchored to a semiconductor surface. Initial studies have indicated that **2** is a promising electrocatalyst for immobilisation as it is able to accept photoelectrons from semiconductor materials including TiO₂ and Ti_{1-x}Zr_xO₂ in aprotic solvents. However issues regarding stability need to be addressed for stable photoelectrochemical CO₂ reduction to occur in protic solvents; a promising approach may be to explore secondary polymer encapsulation as this is known to enhance the stability of immobilised coordination compounds on TiO₂ without a detrimental effect on the electrical properties.³⁸ A key component of this study is a fundamental assessment of the factors controlling charge transfer to molecular electrocatalysts which confirms the effectiveness of the approach of hybrid covalently immobilised molecular/semiconductor system for enabling efficient photoelectron transfer.

Acknowledgements

AJC and JJW acknowledge the EPSRC for a fellowship (EP/K006851/1) and financial support respectively, Prof K. Durose and Dr. R. Treharne for access to the profilometer, Dr. T. D. Veal and Mr. M. Birkett for use of the FTIR. Prof. M. Brust is thanked for the loan of the HMDE. AR thanks the European Commission Marie Curie CIG (PhotoCO₂). JRD, AR and LX thank the ERC project Intersolar for funding.

Notes and references

^a These authors contributed equally to this work

^b Department of Chemistry, Stephenson Institute for Renewable Energy, The University of Liverpool, L69 7ZF, E-mail: a.j.cowan@liverpool.ac.uk

^c Department of Chemistry, Imperial College London, London SW7 2AZ

* Corresponding author

† Electronic supplementary information (ESI) available: Experimental protocols, prolonged CPE, FTIR and UV/vis of films. See DOI: 10.1039/c000000x/

1. J. Qiao, Y. Liu, F. Hong and J. Zhang, *Chem. Soc. Rev.*, 2014, **43**, 631-675.
2. W. Tu, Y. Zhou and Z. Zou, *Advanced Mater.*, 2014, **26**, 4607-4626.
3. T. Yui, Y. Tamaki, K. Sekizawa and O. Ishitani, in *Photocatalysis*, ed. C. A. Bignozzi, Springer Berlin Heidelberg, Editon edn., 2011, vol. 303, pp. 151-184.
4. B. Kumar, J. M. Smieja and C. P. Kubiak, *J. Phys. Chem. C*, 2010, **114**, 14220-14223.
5. B. Kumar, M. Llorente, J. Froehlich, T. Dang, A. Sathrum and C. P. Kubiak, *Annu. Rev. Phys. Chem.*, 2012, **63**, 541-569.
6. S. Sato, T. Morikawa, S. Saeki, T. Kajino and T. Motohiro, *Angew. Chem. Int. Ed.*, 2010, **49**, 5101-5105.
7. S. Chardon-Noblat, M. N. Collomb-Dunand-Sauthier, A. Deronzier, R. Ziessel and D. Zsoldos, *Inorg. Chem.*, 1994, **33**, 4410-4412.
8. T. Hirose, Y. Maeno and Y. Himeda, *J. Mol. Catal. a: Chem.*, 2003, **193**, 27-32.
9. T. Arai, S. Sato, K. Uemura, T. Morikawa, T. Kajino and T. Motohiro, *Chem. Commun.*, 2010, **46**, 6944-6946.
10. T. Arai, S. Sato, T. Kajino and T. Morikawa, *En. Environ. Sci.*, 2013, **6**, 1274-1282.
11. T. M. Suzuki, H. Tanaka, T. Morikawa, M. Iwaki, S. Sato, S. Saeki, M. Inoue, T. Kajino and T. Motohiro, *Chem. Commun.*, 2011, **47**, 8673-8675.
12. K.-i. Yamanaka, S. Sato, M. Iwaki, T. Kajino and T. Morikawa, *J. Phys. Chem. C*, 2011, **115**, 18348-18353.
13. K. Maeda, K. Sekizawa and O. Ishitani, *Chem. Commun.*, 2013, **49**, 10127-10129.
14. K. Sekizawa, K. Maeda, K. Domen, K. Koike and O. Ishitani, *J. Am. Chem. Soc.*, 2013, **135**, 4596-4599.
15. A. Bachmeier, S. Hall, S. W. Ragsdale and F. A. Armstrong, *J. Am. Chem. Soc.*, 2014, **136**, 13518-13521.
16. M. Beley, J. P. Collin, R. Ruppert and J. P. Sauvage, *J. Chem. Soc. Chem. Comm.*, 1984, 1315-1316.
17. E. Fujita, J. Haff, R. Sanzenbacher and H. Elias, *Inorg. Chem.*, 1994, **33**, 4627-4628.
18. J. Schneider, H. Jia, K. Kobiro, D. E. Cabelli, J. T. Muckerman and E. Fujita, *En. Environ. Sci.*, 2012, **5**, 9502-9510.
19. M. Beley, J. P. Collin, R. Ruppert and J. P. Sauvage, *J. Am. Chem. Soc.*, 1986, **108**, 7461-7467.
20. J. L. Grant, K. Goswami, L. O. Spreer, J. W. Otvos and M. Calvin, *J. Chem. Soc. Dalton*, 1987, 2105-2109.
21. C. A. Craig, L. O. Spreer, J. W. Otvos and M. Calvin, *J. Phys. Chem.*, 1990, **94**, 7957-7960.
22. E. Kimura, X. H. Bu, M. Shionoya, S. J. Wada and S. Maruyama, *Inorg. Chem.*, 1992, **31**, 4542-4546.
23. C. Herrero, A. Quaranta, S. El Ghachtouli, B. Vauzeilles, W. Leibl and A. Aukauloo, *Phys. Chem. Chem. Phys.*, 2014, **16**, 12067-12072.
24. J.-P. Petit, P. Chartier, M. Beley and J.-P. Deville, *J. Electroanal. Chem. Interfac. Electrochem.*, 1989, **269**, 267-281.
25. M. G. Bradley and T. Tysak, *J. Electroanal. Chem.*, 1982, **135**, 153-157.
26. J. P. Petit, P. Chartier, M. Beley and J. P. Deville, *J. Electroanal. Chem.*, 1989, **269**, 267-281.
27. J. D. Froehlich and C. P. Kubiak, *Inorg. Chem.*, 2012, **51**, 3932-3934.
28. K. Bujno, R. Bilewicz, L. Siegfried and T. A. Kaden, *J. Electroanal. Chem.*, 1998, **445**, 47-53.
29. B. Bosnich, M. L. Tobe and G. A. Webb, *Inorg. Chem.*, 1965, **4**, 1109-1112.
30. A. Anichini, L. Fabbri, P. Paoletti and R. M. Clay, *Inorg. Chim. Acta*, 1977, **24**, L21-L23.
31. A. J. Morris, G. J. Meyer and E. Fujita, *Acc. Chem. Res.*, 2009, **42**, 1983-1994.
32. S. N. Frank and A. J. Bard, *J. Am. Chem. Soc.*, 1975, **97**, 7427-7433.
33. G. Redmond and D. Fitzmaurice, *J. Phys. Chem.*, 1993, **97**, 1426-1430.
34. E. Topoglidis, T. Lutz, J. R. Durrant and E. Palomares, *Bioelectrochem.* 2008, **74**, 142-148.
35. E. Topoglidis, A. E. G. Cass, B. O'Regan and J. R. Durrant, *J. Electroanal. Chem.*, 2001, **517**, 20-27.
36. D. Bahnemann, A. Henglein, J. Lilie and L. Spanhel, *J. Phys. Chem.*, 1984, **88**, 709-711.
37. A. Reynal, J. Willkomm, N. M. Muresan, F. Lakadamyali, M. Planells, E. Reisner and J. R. Durrant, *Chem. Commun.*, 2014, **50**, 12768-12771.
38. K.-R. Wee, M. K. Brennaman, L. Alibabaei, B. H. Farnum, B. Sherman, A. M. Lapidus and T. J. Meyer, *J. Am. Chem. Soc.*, 2014, **136**, 13514-13517.